Controlling marginally detached divertor plasmas

D. Eldon[1,2]**, E. Kolemen**[2]**, J.L. Barton**[3]**, A.R. Briesemeister**[4]**,
D.A. Humphreys**[1]**, A.W. Leonard**[1]**, R. Maingi**[5]**, M.A. Makowski**[6]**,
A.G. McLean**[6]**, A.L. Moser**[1] **and P.C. Stangeby**[7]

[1] General Atomics, PO Box 85608, San Diego, CA 92186-5608, United States of America
[2] Princeton University, Princeton, NJ 08543, United States of America
[3] Sandia National Laboratories, Livermore, CA 94550, United States of America
[4] Oak Ridge National Laboratory, Oak Ridge, TN 37831, United States of America
[5] Princeton Plasma Physics Laboratory, Princeton, NJ 08540, United States of America
[6] Lawrence Livermore National Laboratory, PO Box 808, Livermore, CA 94550,
United States of America
[7] University of Toronto Institute for Aerospace Studies, Toronto M3H 5T6, Canada

E-mail: eldond@fusion.gat.com

Abstract

A new control system at DIII-D has stabilized the inter-ELM detached divertor plasma state
for H-mode in close proximity to the threshold for reattachment, thus demonstrating the
ability to maintain detachment with minimal gas puffing. When the same control system was
instead ordered to hold the plasma at the threshold (here defined as $T_e = 5\,\mathrm{eV}$ near the divertor
target plate), the resulting T_e profiles separated into two groups with one group consistent with
marginal detachment, and the other with marginal attachment. The plasma dithers between the
attached and detached states when the control system attempts to hold at the threshold. The
control system is upgraded from the one described in Kolemen *et al* (2015 *J. Nucl. Mater.* **463**
1186) and it handles ELMing plasmas by using real time D_α measurements to remove during-
ELM slices from real time T_e measurements derived from divertor Thomson scattering. The
difference between measured and requested inter-ELM T_e is passed to a PID (proportional-
integral-derivative) controller to determine gas puff commands. While some degree of
detachment is essential for the health of ITER's divertor, more deeply detached plasmas have
greater radiative losses and, at the extreme, confinement degradation, making it desirable to
limit detachment to the minimum level needed to protect the target plate (Kolemen *et al* 2015
J. Nucl. Mater. **463** 1186). However, the observed bifurcation in plasma conditions at the outer
strike point with the ion $\boldsymbol{B} \times \nabla \boldsymbol{B}$ drift into the divertor makes this a significant challenge.
If the divertor plasma were to reattach between ELMs, there would be a long (depending
on delays in the gas puff system) window of high heat flux before detachment could be
re-established. Thus, good understanding of detachment behavior near the threshold for
re-attachment is required to properly tune an active control system to maintain ideal divertor
performance without reattaching. The top-of-pedestal electron densities during dithering
across the bifurcation and during stable marginally detached operation are the same within
uncertainty, showing the need for local real-time measurements of the divertor conditions.

Keywords: divertor, tokamak, control

(Some figures may appear in colour only in the online journal)

1. Introduction

Divertor detachment provides a means of reducing peak heat loads on the target surface by increasing the volume of radiating plasma in the divertor and is seen as a requirement for ITER or reactor operation [1, 2]. However, the high plasma densities required for detachment can degrade confinement [2] and produce MARFEs [3], which can lead to problems including disruptions [4]. There are three macro stages of detachment at DIII-D which can be characterized in terms of electron temperature T_e in and near the divertor. In attached operation, T_e just above the target plate is about 10 eV or greater in H-mode with the *X*-point temperature somewhat higher. As density increases, a partially detached condition is achieved, where T_e at the target rapidly falls below 3 eV but T_e around the *X*-point remains close to attached levels. Further increases in density lead to full detachment, where T_e at the *X*-point drops substantially, as shown in figure 1 [5]. This work focuses on T_e due to its direct use in the control system, its role in controlling detachment [6], and its importance for sputtering of the divertor target, but heat flux to the target also decreases significantly in detachment (<5 eV). In deuterium H-modes with $\boldsymbol{B} \times \nabla \boldsymbol{B}$ into the divertor, including the case studied by McLean *et al* [5] and the deuterium plasma case studied in this work, the transitions between the three states are abrupt (see figure 2). The fully attached state suffers from high T_e and heat flux at the target plate, while the fully detached state is prone to poor confinement, MARFEs, and increased risk of radiative collapse. Thus, the partially detached state is most desirable. However, partial detachment occurs in a narrow operating space with dependencies which have yet to be fully determined. This paper will discuss operations near the transition between attached and partially detached operation in DIII-D [7]. The T_e cliff (see figure 2) is used as the boundary between attached plasmas and the start of detachment, and the terms marginally attached and marginally detached are used to define states with T_e very close to the edges of the T_e cliff.

In order to ensure stable, continuous operation in the partially detached scenario, a feedback control algorithm was developed and tested in DIII-D L-mode discharges [1]. Recent improvements to the control system have allowed operation in type-I ELMing H-mode. The control is versatile and can be redeployed to manage new scenarios very quickly. For example, it was recently used to control detachment in a helium plasma. Lacking a suitable reference shot to use for pre-tuning the controller, the required data were collected from a single shot, the tuning parameters were calculated from these data between shots, and the control system was programmed and activated for the next shot (see section 3.2).

The remainder of this paper is organized as follows: section 2 describes the technical details of the control system, the deuterium plasmas used for testing it, and the adaptations needed to operate in helium. Section 3 contains results of operating the control system, including an evaluation of its performance and properties of the divertor plasma on the margins of the transition between partial detachment and re-attachment. Finally, discussion and conclusions are presented in section 4.
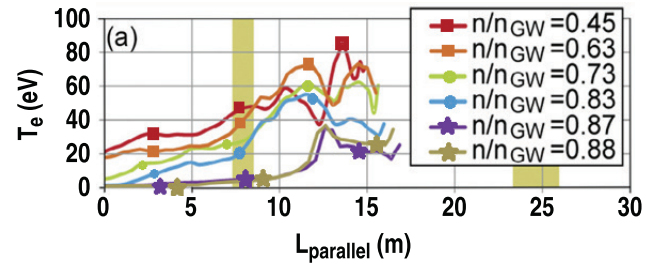

Figure 1. Profiles of T_e versus $L_{parallel}$, the distance along the field from the target plate, averaged over the flux surface range of $\psi_N = 1.000–1.004$. The attached profiles are marked with red and orange squares, partial detached profiles with green and blue circles, and fully detached profiles with purple and brown stars. The vertical shaded regions mark the *X*-point and the outboard midplane. Measurements are from DIII-D's divertor Thomson system [8]. The apparent peaking behavior around $L_{parallel} = 13$ m may be related to poloidal variation in electron pressure reported by Shaffer *et al* [9] (see figure 9 of [9]). Although Shaffer's model detected variation in density, perhaps similar effects influence T_e. There may be other explanations, such as scatter in the measurements. Reprinted from [5], Copyright 2015, with permission from Elsevier.
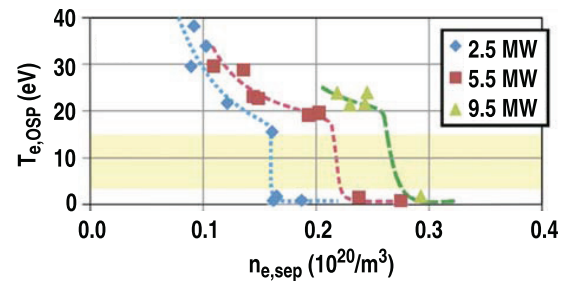

Figure 2. DIII-D divertor T_e from Thomson scattering parameterized against upstream separatrix density for three steps in a power scan, showing the T_e cliff marked by the yellow shaded region. Curves are drawn through the data to guide the eye. Reprinted from [5], Copyright 2015, with permission from Elsevier.

2. Technical details of the control system and experimental setup

2.1. Control algorithm and actuator hardware

The controller exploits DIII-D's unique divertor Thomson scattering (DTS) diagnostic [8] to allow feedback control of gas fueling rate based on local T_e measurements near the target plate. DIII-D's DTS diagnostic samples every 20 ms (50 Hz) and can measure T_e below 1 eV with ~20% error. At higher temperatures (>100 eV), DIII-D's Thomson system (including the divertor subsystem) typically delivers about 5–10% error in T_e and n_e [10]. DTS data are available in real time. ITER will be similarly equipped with a DTS system according to current plans [11]. The key hardware used in the DIII-D control system is shown in figure 3. Data from the selected chord(s) are passed to the plasma control system (PCS) in real time and analyzed to produce T_e and n_e measurements as in the scheme described by Kolemen *et al* [1]. D_α measurements from a filterscope (a photodiode aimed at the plasma through an optical band-pass filter accepting light at the deuterium Balmer alpha line at 656.1 nm and sampled at 20 kHz) [12] are used to detect ELMs, and DTS data taken
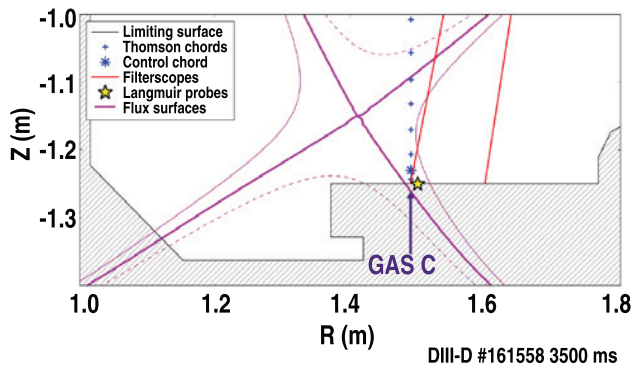
Figure 3. Positions of diagnostics and actuators for the detachment control system in the lower divertor region of DIII-D. Of the filterscope chords shown, the outermost was used for detecting ELMs during detachment as the normally prominent ELM-induced flash of light at the strike point is not as clear in detached plasmas and can actually become inverted in deep detachment. However, both chords were connected to the PCS and available in real time. The location of the Langmuir probe used later (section 3.1.1) is shown as well. Of the available DTS chords, the favored one for use in the control system is marked with an asterisk and reported T_e will be from this chord unless otherwise specified.

during ELMs are rejected. This is necessary because the ELMs transiently change divertor conditions on a timescale that is much faster (~1 ms) than the plasma response to gas commands (~100 ms), and the intra-ELM measurements are not representative of the inter-ELM plasma conditions. Because of the inverse ELM phenomena that is sometimes observed in detachment, a filterscope chord aimed at larger R than the strike point is used (see figure 3). Next, the worst outliers are removed to ensure that the controller does not respond to bad measurements. In real time, outlier rejection is accomplished by the internal χ^2 limits in the Thomson analysis and then by checking against an acceptable range such as 0.1–50 eV. Very low temperatures (<0.1 eV) out of DIII-D's Thomson system are suspicious enough to reject and $T_e > 50$ eV could indicate either a bad datum or simply that the plasma state is outside of the range where the detachment controller has been optimized; either way, the control system should not respond to such a measurement. For post-shot analysis, outliers were detected using thresholds on reduced χ^2 (in the fit to raw Thomson scattering signals) and fractional uncertainty. Finally, the T_e measurements that are admitted by the ELM/outlier filters are RC low-pass filtered and then compared to the requested T_e value. The difference is sent to a PID controller which sets the command voltage at the gas valve, resulting in increased puffing of deuterium into the divertor when the measured T_e is above the request, and decreased puffing when the measurement is below the request. The best starting point seems to be a modified Ziegler–Nichols [13] tuning with proportional gain reduced by 50%. The initial tuning is later improved after seeing the results.

The real time ELM detector works as follows: let D be the intensity of D_α light. D is smoothed with an RC low-pass filter to give S ($\tau = 1$ ms or $\omega_{cut} = 1$ krad s^{-1}). The time derivative of S is smoothed with two different timescales ($\tau_1 = 1$ ms, $\tau_2 = 5$ ms or $\omega_{cut,1} = 1$ krad s^{-1}, $\omega_{cut,2} = 0.2$

krad s^{-1}) to get SD$_1$ and SD$_2$. Each of the three quantities (D–S), SD$_1$, and SD$_2$ is compared to its own threshold, and if any of the three exceeds its threshold, an ELM is registered. The first component, where the difference of D and S is used, is similar to the difference of Gaussians edge detection scheme. The SD$_1$ and SD$_2$ components help find the edges where the ELM starts and stops. The advantages of this technique are that it can find the whole ELM and not just its peak, and that it can detect a mixture of different ELM sizes and timescales, as seen in figure 4. These features are necessary for properly rejecting ELMy data. This ELM detection logic has been adapted into a set of OMFIT [14] scripts for post-shot analysis needs.

2.2. Experimental setup (deuterium)

DIII-D discharges were operated in a lower single null configuration with the strike point on the shelf near the Thomson scattering measurement location (see figure 3) with the following key parameters: plasma current $I_p = +1.27$ MA, toroidal field $B_T = -2.05$ T, line averaged electron density $\langle n_e \rangle = 8.8$–$10.1 \times 10^{19}$ m^{-3}, normalized beta $\beta_N = 1.3$–1.5, major radius $R = 1.73$ m, and minor radius $a = 0.60$ m. The plasmas were fueled with deuterium from a gas inlet in the main chamber during startup with peak flow rate of 20 Pa m^3 s^{-1}, and then this source was set to a constant flow of 5 Pa m^3 s^{-1} when the detachment control system was activated using the gas inlet in the divertor (GAS C) as shown in figure 3. The typical delay between changes in gas commands to this port (when loaded with D$_2$) and responding changes in divertor T_e is ~100 ms. The deuterium gas flow into the divertor during feedback control varied significantly as conditions evolved and requests changed (see figure 5), but was on the order of 1.5 Pa m^3 s^{-1}.

2.3. Extension to helium

The same control logic as described above was used to control detachment in helium plasmas using nitrogen instead of deuterium gas puffing into the divertor (again through the GAS C port in figure 3). The controller is tuned by adjusting the PID gains and smoothing timescales for the P, I, and D terms, and good performance requires good tuning. As helium shots in DIII-D are much less common than deuterium, a previous case in a similar scenario was not available for use as a guide in preparing an initial tuning setup. Instead, the helium control experiment began with a tuning data acquisition shot where the gas valve was opened to a constant flow rate for 400 ms and then closed again. A tuning calculator utility that was prepared for the deuterium experiment was used to read in the plasma response to the gas command, fit it to a first order plus dead time (FOPDT) model, and suggest initial gain settings based on a modification of the Ziegler–Nichols PID scheme [15]. This initial guess produced a functional controller which was refined over the next few shots to improve performance. Nitrogen was used as the gas under feedback control as it was hoped that it could be removed by the cryopumps, unlike
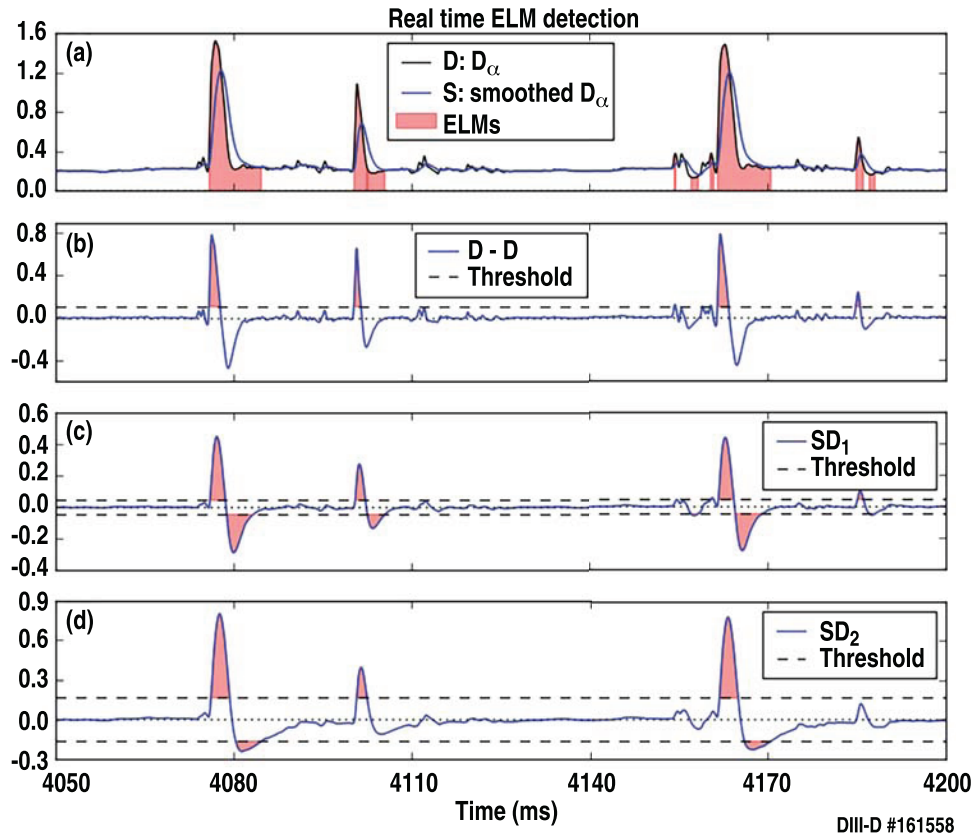
Figure 4. Results of real time ELM detection scheme operating on D_α measurements. (*a*) The history of D_α measurements D from the filterscope chord ending near 1.6 m (see figure 3) is shown by the black curve, and the RC lowpass filtered version S by the blue curve. Red shading indicates times when an ELM has been detected. (*b*) Times when $(D–S) >$ threshold are marked as ELMy. (*c*) Times when the magnitude of the smoothed derivative (SD$_1$) exceeds a threshold are also marked as ELMy. (*d*) The derivative is smoothed with a longer timescale and its magnitude compared to yet another threshold. Red shading on ((*b*)–(*d*)) indicates when a single test has indicated an ELM whereas red shading on (*a*) indicates when any of the tests from (*b*) to (*d*) indicates an ELM and is the final result that is used to reject data. The ELMs are reported as lasting longer than would be inferred from the D_α trace because the thresholds on SD$_1$ and SD$_2$ are probably too small. However, this has the effect of rejecting more data in early ELM recovery when large changes are more likely, so it is acceptable and perhaps beneficial for this application. The ELM detector used for offline analysis in this work is based on the same principles, but is more complicated and is tuned more carefully with the goal of describing the ELMs more so than aiding the control system.

helium. However, pumping efficiency appears to be quite low, as shown in section 3.2.

3. Experimental results

3.1. Control performance and detachment properties in deuterium H-mode

With the addition of the ELM detector described in section 2.1 to the controller described by Kolemen *et al* [1], it was possible to feed back on the inter-ELM T_e during type-I ELMing H-mode. This control was effective at delivering results close to the requested temperature if the request was outside of a 'T_e cliff' or rapid transition where stable operation was not achieved (cliff refers to a discontinuity in the plot of divertor T_e versus density; see figure 2 [5]). If the request was within the cliff, the requested T_e was found to be delivered on average, but with jumps across the cliff. For example, figures 5(*a*) and (*b*) shows a case where $T_e = 2.0$ eV was requested and the actual T_e is about 1 eV for most of the shot. As this is too low, the controller reduces puff rate in order to let T_e rise. At about 3 s, T_e does come up, but then it jumps

across the cliff to around 10 eV. The controller responds by increasing gas puffing and pulls T_e back to the cold side of the cliff, or about 1 eV again. The puff rate is decreased slowly to try to get to the request of 2.0 eV, which causes another jump to the hot side of the cliff at about 4.5 s, which is met with a slight increase in puffing to bring T_e back down. Reducing the request to 1.0 eV should avoid the occasional jumps in T_e; this could be confirmed with further testing. Another shot (not shown) with T_e request = 12 eV (hot edge of the cliff) delivered mostly hot (10–20 eV) results with a few brief dips down to 1 eV. When the T_e request was set to the middle of the cliff (5 eV), measured T_e jumped up and down across the band, as seen in figures 5(*c*) and (*d*).

When comparing the marginally partially detached case (request = 2.0 eV; only occasional excursions to high T_e as seen in figure 5(*a*)) to the dithering case (request = 5.0 eV; frequent excursions to high T_e figure 5(*c*)), it is found that the pedestal electron density is about the same, as shown in figure 6. This shows that the control system can deliver a partially detached solution that occurs at roughly the same upstream parameters as the dithering case: the minimum density required for partial detachment can be produced. The
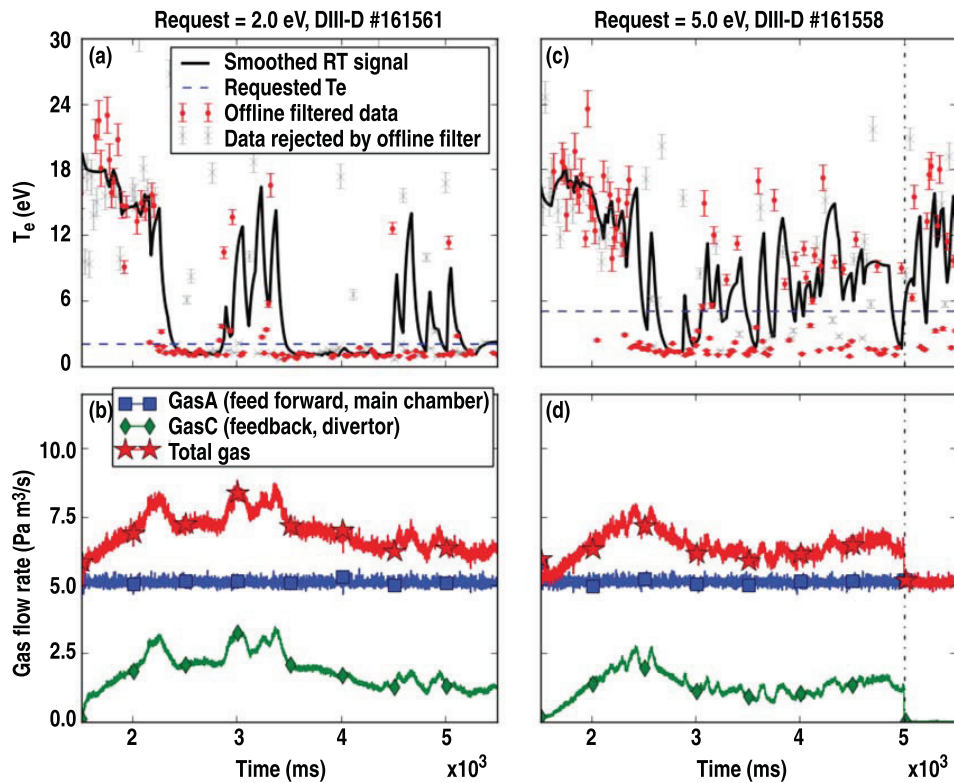
Figure 5. Measured versus requested T_e at the divertor target versus time ((*a*) and (*c*)) and gas flow rates ((*b*) and (*d*)) for request = 2 eV (detached) ((*a*) and (*b*)) and request = 5 eV (dithering) ((*c*) and (*d*)). (*a*) and (*c*) Black: time history of real time filtered and RC low-pass smoothed Thomson T_e measurements. Red points: post-shot filtered and cleaned up T_e measurements; these agree well but not perfectly with the real time filtering as the post-shot filter is more complex and can be inspected and fine-tuned more easily. Blue dashed line: requested T_e value. (*b*) and (*d*) Constant gas puff into the main chamber to maintain baseline density (blue squares), feedback controlled gas puff into divertor (green diamonds), and total gas puff (red stars).

average pedestal densities for the detached and dithering cases between 3000 and 5000 ms (after ~stationary operation has been reached) are 9.21 ± 0.12 and $9.09 \pm 0.12 \times 10^{19}$ m^{-3}, giving a difference of $1.4 \pm 1.9\%$. In contrast, the attached solution (also in figure 6) occurs at $8.25 \pm 0.11 \times 10^{19}$ m^{-3}, or $10.3 \pm 1.7\%$ lower $n_{e,ped}$ than the average of the detached and dithering cases. All three cases had the same constant 5 Pa m^3 s^{-1} gas puff into the main chamber. The divertor puffing rate was under feedback control and varied over time (as seen in figure 5), but typical rates were about 0.5, 1, and 2 Pa m^3 s^{-1} for the attached, dithering, and partially detached cases. By design, full detachment was not reached in these experiments: figure 1 [5] shows a jump in X-point T_e between partial and full detachment, and the measured T_e of $\gtrsim 15$ eV at the X-point height is consistent with partial detachment and attachment rather than full detachment (note: the array of Thomson measurements does not actually go through the X-point itself, but T_e at the same height as the X-point but larger R should give a reasonable rough estimate; see figure 3(*a*) of McLean *et al* [5] for 2D variation in T_e in the divertor).

The dithering case is interesting because it provides insight into whether or not a stationary solution in the T_e cliff exists, and the answer appears to be no. If a solution existed but the control scheme was simply not capable of stabilizing it, T_e values should be expected to cluster around the request point, albeit with significant noise. Instead, there is a distribution with two groups representing the top and bottom of
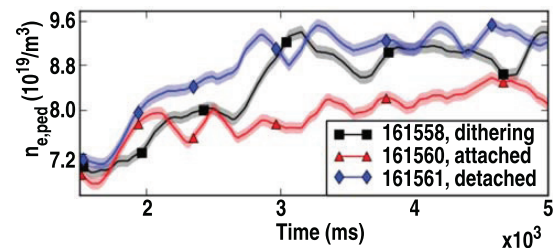

Figure 6. Comparison of upstream pedestal density for different detachment conditions with control starting at 1.5 s. Pedestal density is calculated from automatic tanh fits [16] to Thomson scattering [10] and is filtered to remove measurements taken during ELMs. The control setting for the detached case (blue diamonds, T_e request = 2.0 eV) leads to more aggressive initial gas puffing than the dithering case (black squares, T_e request = 5.0 eV), but both of these cases have reached about the same density by 3 s. The attached case (red triangles, T_e request = 12.0 eV) stays at lower density.

the 'T_e cliff', as seen in figure 7. There is a cluster of values from 8 to 20 eV, and also a cluster near 1–2 eV. The cliff is not completely empty, but this can be explained by the finite time required for T_e to change from ~1 eV to ~10 eV and by random fluctuations in the SOL. The Thomson system averages signal over only about 10 ns (the laser pulse length), meaning that it captures practically instantaneous snapshots of T_e and so, in the presence of fluctuations, it should occasionally capture extrema.
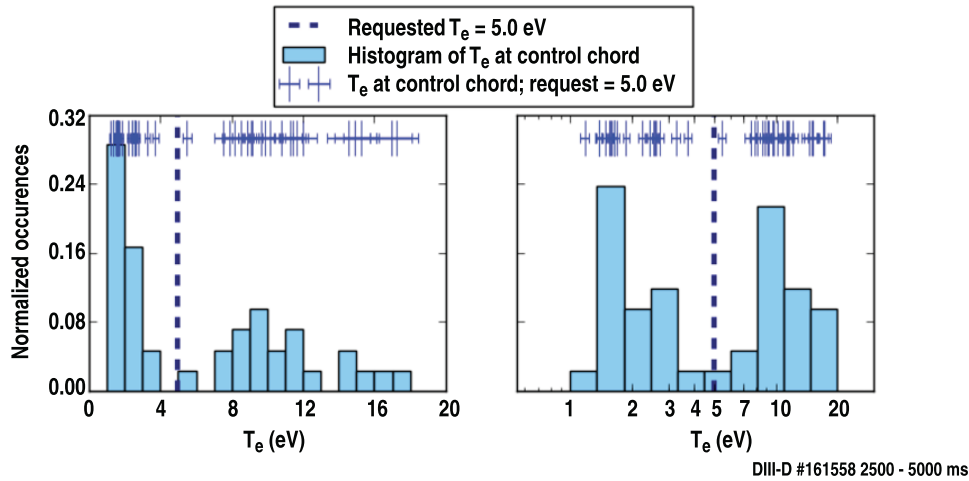
Figure 7. Histogram (bars) of T_e measurements (symbols) at the divertor target (see figure 3) during control with a request in the middle of the cliff (dashed line), shown with linear (left) and logarithmic (right) X-axis scaling. The data separate into two groups around 1–3 eV and 8–20 eV with a sparse region near the requested value. The logarithmic bin spacing in the right panel is useful for visualization because of the difference in width of the two groups; presumably the group widths differ because higher temperature plasmas experience greater fluctuations in T_e, or DTS uncertainty and thus scatter in measurements is higher (this can be seen from the plot where error bars are roughly constant width in the right panel but get wider at higher T_e in the left panel), or both. DTS uncertainty is higher at higher temperature only because density is lower (see figure 12 for correlation between n_e and T_e) and thus signal to noise is lower.
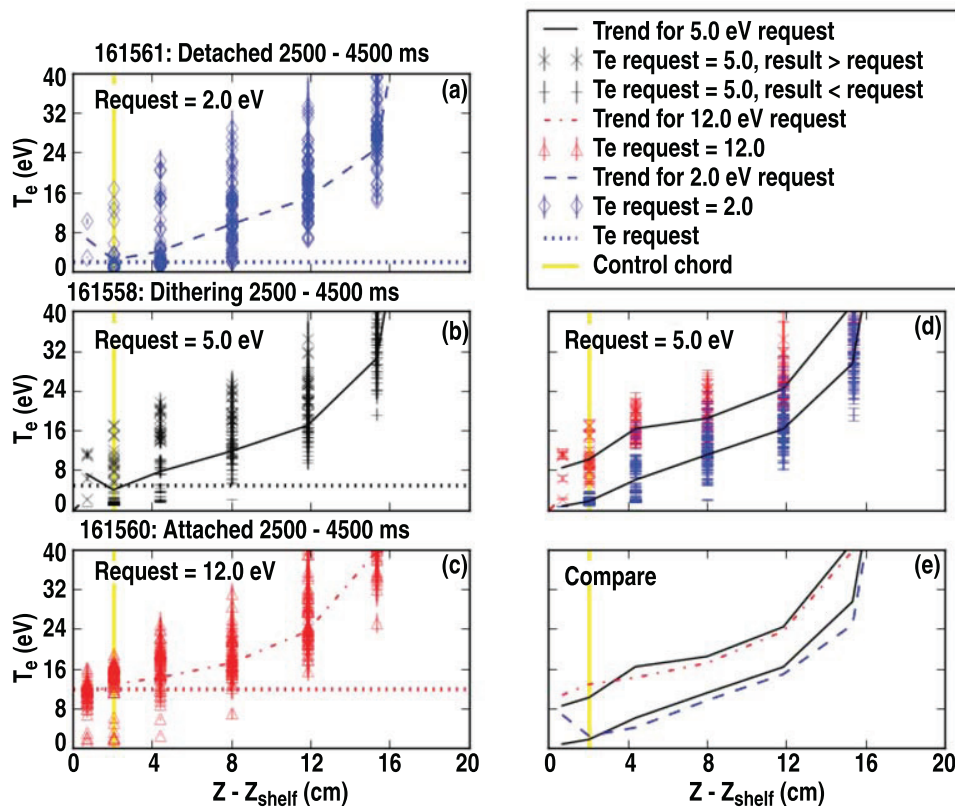

Figure 8. Profiles of electron temperature versus height above the shelf for three requested T_e values representing detachment, attachment, and dithering across the T_e cliff. See figure 3 for the relationship between the Thomson measurement locations and the magnetic flux surfaces. The lowermost Thomson chord (left of the plot range, $Z - Z_{shelf} = 0.7$ cm) was not used for control due to the impact of stray light from the edges of the laser hole (see the sparsity of measurements for the left-most chord in (*a*)); instead the next lowest chord at $Z - Z_{shelf} = 2$ cm was used (marked by the dashed green vertical line). Three shots are shown: (*a*) request = 2 eV, plasma stayed detached most of the time, (*b*) request = 5 eV, dithering detachment/re-attachment, and (*c*) request = 12 eV, plasma stayed attached most of the time. Trends are obtained by weighted average of all the data from each chord. The trendlines in all three cases ((*a*)–(*c*)) are consistent with the requests to the controller (they go through the intersection of the dotted green lines). As T_e at the control chord in (*b*) is jumping across the T_e cliff, we separate the data in (*b*) into two groups according to $T_e >$ request or $T_e <$ request and plot these with separate trendlines in (*d*). (*e*) Compares the trendlines from (*a*) and (*c*) to those in (*d*), showing that the dithering shot is jumping between the T_e profiles observed in the two steady shots at the hot and cold edges of the cliff, and that the entire profile jumps rigidly between states.
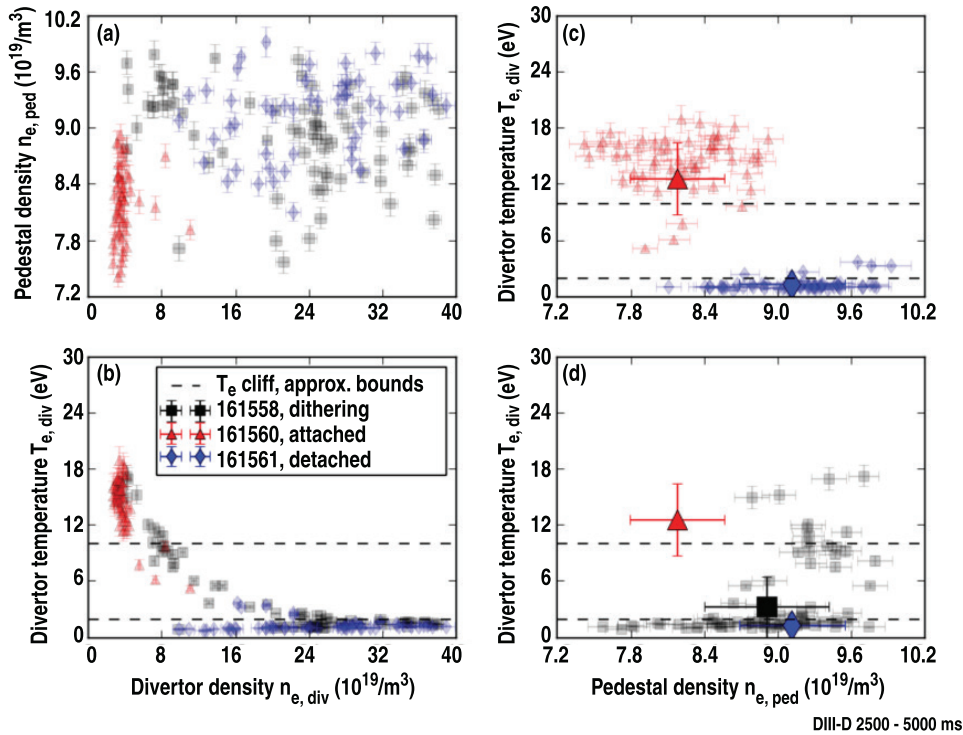
Figure 9. Upstream pedestal density (*a*) and divertor T_e (*b*) versus divertor n_e, showing that (*a*) divertor density can vary widely for the same pedestal density. (*c*) Divertor T_e versus upstream n_e for the steady attached (red triangle) and detached (blue diamond) cases with time averaged values marked with larger, darker symbols (compare with top/bottom of cliff in figure 2). (*d*) Divertor T_e versus upstream n_e for the dithering case with time averaged value marked with a larger darker square and averages from (*c*) overlaid for reference; note that the black squares do not trace out the path suggested by the red triangle, the blue diamond, and figure 2. Dashed lines are drawn at 2 and 10 eV for reference.

Recent advances in scrape off layer models [17–19] describe a bifurcation at detachment with properties similar to the observed T_e cliff, with some models [17, 18] suggesting that drifts ($\mathbf{E} \times \mathbf{B}$ and $\mathbf{B} \times \nabla\mathbf{B}$) play a key role. These models are consistent with our difficulty in achieving stationary operation in the middle of the T_e cliff for the given experimental configuration.

The dithering case is also interesting because it shows us that it is not just T_e at the target that is jumping up and down the cliff, but that the entire divertor T_e profile is moving up and down, as seen in figure 8. Figure 8(*a*) shows T_e versus vertical height above the target plate for the detached (request = 2.0 eV) case, 8(*b*) shows the dithering (request = 5.0 eV) case, and 8(*c*) shows the attached (request = 12.0 eV) case. Given the separation of T_e measurements in the dithering case into two groups (see figure 7), we can separate the measurements in figure 8(*b*) based on whether T_e at the control chord is above or below the request; the result is plotted in figure 8(*d*). For each set of data, we calculate the weighted average T_e (weighting by the inverse variance $\sigma_{T_e}^{-2}$) for each chord and connect the averaged points with the dashed blue, solid black, and dashed-dotted red curves. Figure 8(*e*) shows the curves for the attached and detached cases (copied from (*a*) and (*c*)) along with two curves for the two groups of dithering data (copied from (*d*)). Figure 8(*e*) shows that data from the 'hot' half of the dithering set form a profile that is consistent with the profile from the attached case, and the 'cold' dithering data form a profile consistent with the detached case.
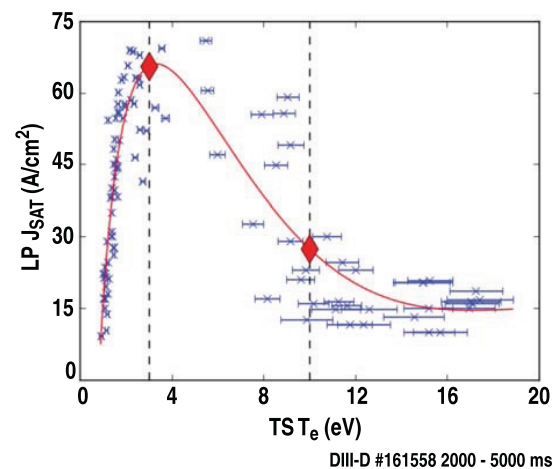

Figure 10. Saturation current density (J_{sat}) from Langmuir probes versus electron temperature (T_e) from divertor Thomson scattering at the control chord. The approximate edges of the T_e cliff are marked by red diamonds; note the limited data between the diamonds (compare with figure 7).

Figure 9 demonstrates the importance of local measurements in the divertor. Figure 9(*a*) shows that divertor density can vary widely for the same pedestal density and figure 9(*b*) shows that there is no appearance of a T_e cliff when T_e is plotted versus local density instead of upstream density. This emphasis on local changes in the divertor fits well with observations at NSTX, on which device detachment seems to require local divertor gas injection and is not achieved with
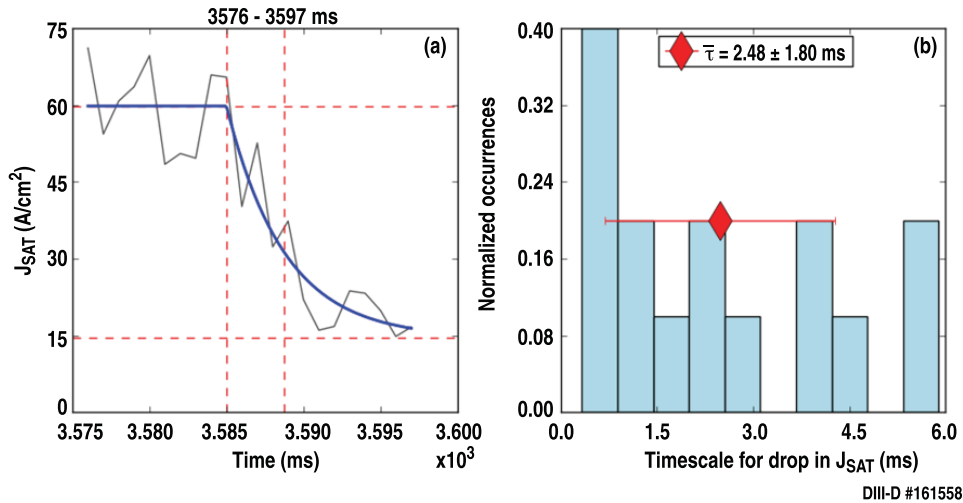
Figure 11. (*a*) Example of exponential fit to J_{sat} versus time during re-attachment; measured J_{sat} is shown in black while the fit is shown in blue. (*b*) Histogram of results from timescale fits to several reattachment events. The selected events were those which occurred during quiescent periods between large ELMs. One outlier ($\tau = 12$ ms) out of 16 measurements was discarded, giving an average timescale of 2.48 ms with standard deviation of 1.8 ms (with the outlier, the average is 3.26 ± 2.89 ms). The average value and standard deviation are marked on the plot by the red diamond with error bars.
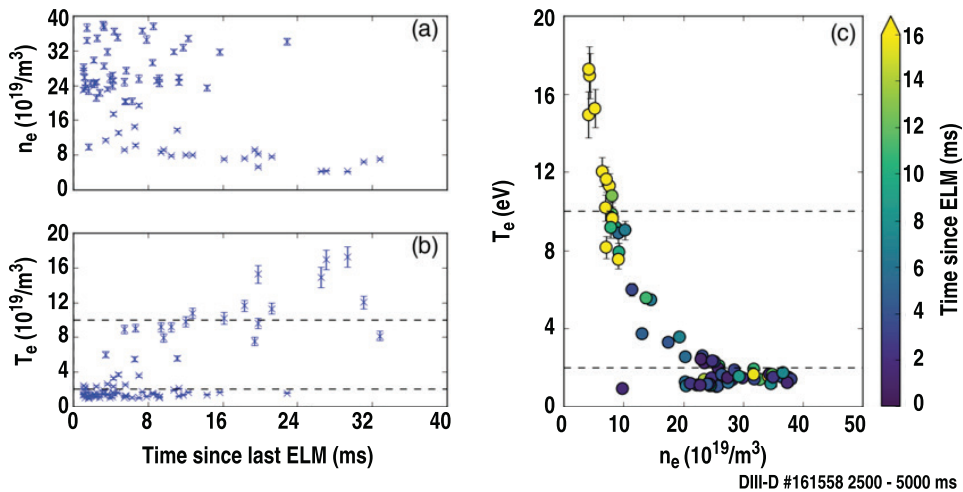

Figure 12. Changes in divertor T_e and n_e versus time since the end of the last ELM. T_e and n_e are measured by DTS at the control chord shown in figure 3. (*a*) and (*b*): n_e and T_e versus time since last ELM. (*c*): T_e versus n_e with symbols colored by time since last ELM. Dashed horizontal lines mark the approximate edges of the T_e cliff at 2 and 10 eV. Attached samples typically occur longer after ELMs. The scatter the length of the detached phase after ELMs probably results from variability in the ELMs themselves and adjustments to gas flow made by the control system. In particular, the single cold, dense point occurring 24 ms after the last ELM (yellow mark at bottom right of (*c*)) was measured at 2936 ms, just after a period of aggressive puffing when T_e stayed cool for about half a second without dithering (see figures 5(*c*) and (*d*)).

global changes in density alone [20]. The cliff is still present in this data set as the sparse region between the high T_e/low n_e group and the low T_e/high n_e group in figure 9(*b*) (~3–8 eV range). Also, considering divertor T_e versus upstream n_e (figure 9(*c*)), we see that the time averaged values for the steady attached and detached cases could plausibly be at the top and bottom of the T_e cliff (see figure 2). However, when we examine data from the dithering case in figure 9(*d*), we see that the scatter in T_e and n_e values does not fall along the curve suggested by figure 2. This may be because upstream and divertor density fluctuations during dithering are not synchronized (see figure 9(*a*)). In this case, the relationship in figure 2 only works if divertor and upstream density have time to equilibrate; clearly, upstream density is not directly

driving detachment transitions and we should focus on local measurements.

3.1.1. Timescale of the transition across the T_e cliff and ELM interactions.

While Thomson scattering samples too infrequently to be used to determine the timescale of the detachment transition, we find the changes in T_e across the cliff (~1–10 eV) do correlate with changes in the ion saturation current density (J_{sat}) measured by Langmuir probes [21] as seen in figure 10. Accordingly, the timescale for the jump across the T_e cliff can be measured by timing the drop in J_{sat} on the 'hot' side of the J_{sat} rollover. This timing is accomplished by fitting a decaying exponential to J_{sat} versus time using
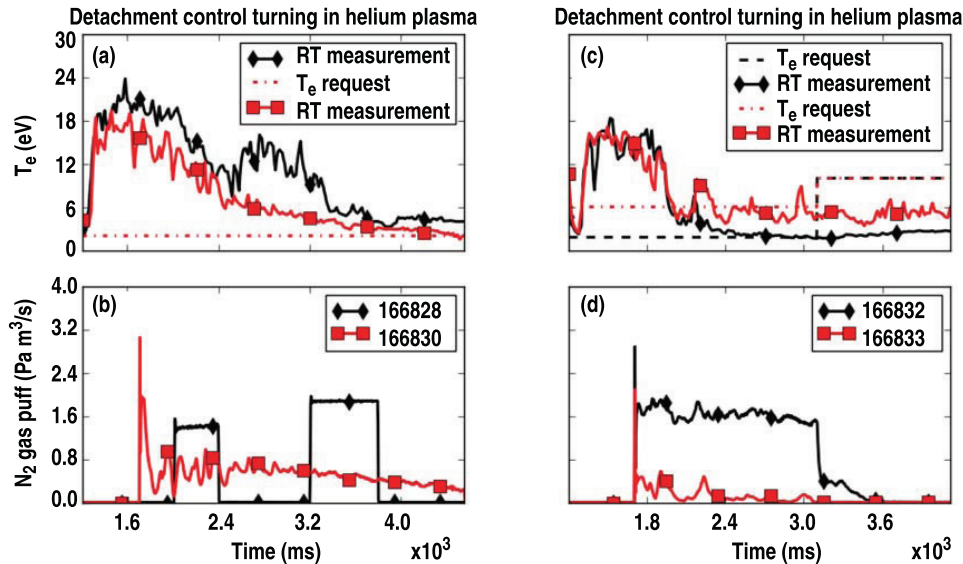
Figure 13. Initial deployment of the detachment controller in a new scenario ((*a*) and (*b*)) and performance of the feedback detachment controller with nitrogen puffing into helium plasma ((*c*) and (*d*)). (*a*) and (*c*) Real time temperature measurements (solid) and requested values (dashes); the request in (*c*) is increased in the latter half of the flattop. (*b*) and (*d*) N$_2$ gas flow rates; the gas flow in 166828 (black in (*a*)) was the tuning data acquisition shot and was the only one not under feedback control. The initial spike in gas flow is added to ensure that the valve does not stick closed when starting with small flow commands.

$J_{sat} = B - A \exp(-(t - t_0)/\tau)$ with an example result shown in figure 11(*a*) (dashed red lines show $B, B - A, t_0, t_0 + \tau$). By performing this exponential fit on several quiescent time windows between ELMs in the dithering shot (161558), we find an average timescale of 2.48 ± 1.8 ms with a histogram of measurements shown in figure 11(*b*). At the conclusion of large ELMs, the divertor plasma typically recovers into a detached state and then may reattach during the subsequent quiescent window. Groups of small ELMs between large ELMs are associated with J_{sat} remaining mostly high, indicating detached conditions.

The observed dithering between attachment and detachment may be a symptom of the ELM cycle in a plasma at the edge of detachment. Starting from a marginally attached plasma, an ELM brings a pulse of power and particles into the divertor. The heat dissipates quickly, leaving behind particles which drain more slowly, so the plasma recovers from the ELM into a detached state. Later, the extra particles drain out of the divertor and it reattaches. The next large ELM repeats the cycle. Figure 12 shows how the ELM cycle drives changes in divertor T_e and n_e: figure 12(*a*) shows density to be highest just after an ELM with a drop after 5–10 ms. Figure 12(*b*) shows low T_e shortly after an ELM with an increase after 5–10 ms. This change in n_e and T_e (which is the jump across the cliff) happens quickly, in the 2.5 ms timescale reported above. Variation in ELM size and character as well as modulations in gas puff by the control system could easily cause variation in the beginning of the transition relative to the last ELM, which is why there is so much scatter in 12(*a*) and (*b*). Figure 12(*c*) shows T_e versus n_e with symbols colored by time since the last ELM; the points at the high T_e (attached) end of the curve occur at a longer time since the last ELM. Again, note the clustering of data near the ends of the curve with a sparse region near 5 eV. The sparse region is the T_e cliff and it is

sparse because the transition is fast. This type of interaction between detachment and ELMs has been suggested by modelling work in DIII-D geometry before [22].

This picture of the interaction between ELMs and detachment can explain why so many transitions are observed, but it does not explain why the jump across the T_e cliff is so fast. Recent modelling work [17, 18, 23] presents a possible answer: with $\boldsymbol{B} \times \nabla \boldsymbol{B}$ into the divertor, there is, at low density, an $\boldsymbol{E} \times \boldsymbol{B}$ drift from the outer strike point into the private flux region which provides a particle sink. This drift weakens as local density increases, meaning that increasing density can feed back on itself by disabling one of its own sinks. This mechanism should work in both directions, with decreasing density allowing the $\boldsymbol{E} \times \boldsymbol{B}$ driven particle sink to recover and drive further decreases (this is the direction shown in figure 13). This could explain why jumps across the T_e cliff are rapid: they are also jumps across a particular n_e range where this feedback may occur. Future work could test this hypothesis by running the detachment controller with $\boldsymbol{B} \times \nabla \boldsymbol{B}$ out of the divertor, in which case the T_e cliff is expected to vanish because $\boldsymbol{E} \times \boldsymbol{B}$ between the private flux region and outer divertor goes the other way and so increasing density would weaken a particle source.

3.2. Helium results

Initial tuning of the detachment controller in helium was accomplished using the procedure described in section 2.3, now relying on nitrogen puffing, and as shown in figures 13(*a*) and (*b*). The response of T_e to two square pulses of gas was measured (black shot #166828) and used to calculate the initial PID gains, which were applied to the next good shot (red shot #166830). Thus, DIII-D demonstrates the ability to rapidly (between shots) redeploy existing controls to new situations with limited prior information.

While the initial tuning did eventually achieve detachment, it approached the request T_e slowly and so the tuning was refined on subsequent shots to improve performance. After an initial delay of about 130 ms, shot 166830 approached the requested T_e of 1.8 eV with an e-folding timescale of 800 ms. For shots 166831 and 166832, the timescale to approach the request of 2.0 eV was about 200 ms.

On shot 166833, the T_e request was raised to 6.0 eV to test whether the controller would overshoot to lower temperatures, which it did not. Shots 166831–166833 featured a step up in T_e request in the latter half of the current flat-top to test whether the nitrogen could be cryo-pumped fast enough to raise the divertor T_e, but it was found that T_e does not increase quickly and the shot ends with T_e near the initial, lower request value. Figures 12(*c*) and (*d*) show the results of the 'overshoot' and 'lower-then-increase tests'. Figure 13(*c*) also shows that requesting $T_e = 6.0$ eV does not provoke jumps in T_e between detached and attached behavior. That is, there is no T_e cliff in helium L-mode, which is consistent with past results and distinct from deuterium H-mode (section 3.1).

4. Conclusions

DIII-D's detachment control system has been upgraded to work in type-I ELMing H-mode and is able to adjust gas puffing rates to control the electron temperature T_e at the outer divertor target. There is, however, a 'cliff' in T_e where stationary operation was not achieved in deuterium. The clustering of T_e measurements into two groups, above and below the cliff, indicates that there is a physical mechanism preventing stationary operation in the cliff. Fortunately, the cold edge of the cliff appears to offer an attractive partially detached solution, and the control system does a good job of holding T_e there. The T_e cliff is consistent with past observations in deuterium H-mode with $\boldsymbol{B} \times \nabla \boldsymbol{B}$ into the divertor [5]. The control system is able to make small adjustments based on local (divertor) measurements to select between partially detached and dithering attached/partially detached cases where upstream pedestal density is nearly indistinguishable, emphasizing the importance of local measurements for controlling divertor detachment. The control system is capable of holding the divertor plasma at the detachment threshold so that modulations in particle balance during the ELM cycle stimulate many transitions between attachment and partial detachment, which allows study of the transition and its relationship with the ELM cycle. Finally, the control system comes with a utility package that allows rapid re-deployment to new scenarios, as shown by between-shot re-tuning to function in a helium plasma.

Acknowledgments

References

[1] Kolemen E. *et al* 2015 Heat flux management via advanced divertor configurations and divertor detachment *J. Nucl. Mater.* **463** 1186

[2] Leonard A.W., Mahdavi M.A., Lasnier C.J., Petrie T.W. and Stangeby P.C. 2012 Scaling radiative divertor solutions to high power in DIII-D *Nucl. Fusion* **52** 063015

[3] Lipshultz B., La Bombard B., Marmar E.S., Pickrell M.M., Terry J.L., Watterson R. and Wolfe S.M. 1984 MARFE: an edge plasma phenomenon *Nucl. Fusion* **24** 977

[4] Gao X. 2000 MARFE phenomena in the HT-7 tokamak *J. Nucl. Mater.* **279** 330

[5] McLean A.G. *et al* 2015 Electron pressure balance in the SOL through the transition to detachment *J. Nucl. Mater.* **463** 533

[6] Loarte A. *et al* 1998 Plasma detachment in JET Mark I divertor experiments *Nucl. Fusion* **38** 331

[7] Hill D.N. and the DIII-D Team 2013 DIII-D research towards resolving key issues for ITER and steady-state tokamaks *Nucl. Fusion* **53** 104001

[8] Carlstrom T.N., Hsieh C.L., Stockdale R., Nilson D.G. and Hill D.N. 1997 Initial operation of the divertor Thomson scattering diagnostic on DIII-D *Rev. Sci. Instrum.* **68** 1195

[9] Schaffer M.J. 2001 $E \times B$ circulation at the tokamak divertor X point *Phys. Plasmas* **8** 2118

[10] Eldon D. *et al* 2012 Initial results of the high resolution edge Thomson scattering upgrade at DIII-D *Rev. Sci. Instrum.* **83** 10E343

[11] Mukhin E.E. *et al* 2012 The ITER divertor Thomson scattering system: engineering and advanced hardware solutions *J. Instrum.* **7** C02063

[12] Colchin R.J., Hillis D.L., Maingi R., Klepper C.C. and Brooks N.H. 2003 The filterscope *Rev. Sci. Instrum.* **74** 2068

[13] Ziegler J.G. and Nichols N.B. 1942 Optimum settings for automatic controllers *Trans. ASME* **64** 759

[14] Meneghini O. *et al* 2015 Integrated modeling applications of tokamak experiments with OMFIT *Nucl. Fusion* **55** 083008

[15] Kolemen E., Gates D.A., Rowley C.W., Kasdin N.J., Kallman J., Gerhardt S., Soukhanovskii V. and Muller D. 2010 Strike point control for the National Spherical Torus Experiment (NSTX) *Nucl. Fusion* **50** 105010

[16] Groebner R.J. *et al* 2001 Progress in quantifying the edge physics of the H mode regime in DIII-D *Nucl. Fusion* **41** 1789

[17] Rognlien T.D., McLean A.G., Fenstermacher M.E., Groth M., Jaervinen A.E., Joseph I., Lasnier C.J., Meyer W., Porter G.D. and Umansky M.V. 2017 Comparison of 2D simulations of detached divertor plasmas with divertor Thomson measurements in the DIII-D tokamak

Nucl. Mater. Energy at press (https://doi.org/10.1016/j.nme.2016.12.002)

[18] Järvinen A.E. *et al* 2017 Interpretations of the impact of cross-field drifts on divertor flows in DIII-D with UEDGE *Nucl. Mater. Energy* at press (https://doi.org/10.1016/j.nme.2016.11.014)

[19] Krasheninnikov S.I. and Smolyakov A.I. 2016 Current convective instability in detached divertor plasma *Phys. Plasmas* **23** 092505

[20] Soukhanovskii V.A. 2009 Divertor heat flux mitigation in the National Spherical Torus Experiment *Phys. Plasmas* **16** 022501

[21] Watkins J.G., Taussig D., Boivin R.L., Mahdavi M.A. and Nygren R.E. 2008 High heat flux Langmuir probe array for the DIII-D divertor plates *Rev. Sci. Instrum.* **79** 10F125

[22] Hogan J., Colchin R., Coster D., Baylor L., Fenstermacher M., Groth M. and Wade M. 2003 Modeling of ELM events and their effect on impurity enrichment *J. Nucl. Mater.* **313** 1221

[23] Järvinen A.E. *et al* 2016 Investigations of the impact of cross-field drifts on divertor detachment in DIII-D with UEDGE *Proc. 43rd European Physical Society Conf. on Plasma Physics (Leuven, Belgium, 4–8 July 2016)* (https://kuleuvencongres.be/eps2016)